(Van Nostrand, New York, 1948).
[66]H. Greenstein, Phys. Rev. 175, 438 (1968).
[67]F. Aronowitz, J. Appl. Phys. 41, 2453 (1970).
[68]F. Aronowitz, Phys. Rev. 139, A635 (1965).
[69]Yu. L. Klimontovich, P. S. Landa, and E. G. Larion-tsev, Zh. Eksper. i Teor. Fiz 52, 1616 (1967) [Sov. Phys. JETP 25, 1076 (1967)].
[70]C. Whitney, Phys. Rev. 181, 535 (1969).
[71]K. Takata, Japan J. Appl. Phys. 11, 699 (1972).
[72]A. P. Kazantsev, S. G. Rautian, and G. I. Surdutovich, Zh. Eksper. i Teor. Fiz. 54, 1409 (1968) [Sov. Phys. JETP 27, 756 (1968)].
[73]V. S. Letokhov, Zh. Eksper. i Teor. Fiz. 54, 1244 (1968) [Sov. Phys. JETP 27, 665 (1968)].
[74]V. S. Letokhov and B. D. Pavlik, Kvant. Elektron. 1, 53 (1971) [Sov. J. Quantum Electron. 1, 36 (1971)].
[75]H. Greenstein, J. Appl. Phys. 43, 1732 (1972).
[76]E. M. Garmire and A. Yariv, IEEE J. Quantum Electron. 3, 222 (1967).
[77]L. W. Davis, Phys. Rev. A 5, 2594 (1972).
[78]T. W. Hänsch, M. D. Levenson, and A. L. Schawlow, Phys. Rev. Lett. 26, 946 (1971).
[79]W. Culshaw, Phys. Rev. 164, 329 (1967).
[80]K. Uehara and K. Shimoda, Japan J. Appl. Phys. 4, 921 (1965).
[81]V. M. Tatarenkov, A. N. Titov, and A. V. Uspenskii, Opt. Spektrosk. 28, 572 (1970) [Opt. Spectrosc. 28, 306 (1970)].
[82]K. Shimoda and K. Uehara, Japan J. Appl. Phys. 10, 460 (1971).
[83]N. G. Basov, O. N. Kompanets, V. S. Letokhov, and V. V. Nikitin, Zh. Eksper. i. Teor. Fiz. 59, 394 (1970) [Sov. Phys. JETP 32, 214 (1971)].
[84]Recall, however, that we have assumed $\alpha\lambda$ small in the derivation of (120), and that the Doppler limit requires the saturation broadening to remain small compared to the Doppler width.
[85]S. Autler and C. H. Townes, Phys. Rev. 100, 703 (1955).
[86]*CRC Standard Mathematical Tables*, 14th ed., edited by S. M. Selby and B. Girling (The Chemical Rubber Co., Cleveland, 1964), p. 393.
[87]Note that this corresponds to setting $R_3 = 0$ and $T_2 = (1-\lambda)(F_1^- - \lambda F_1^+)$, i.e., retaining part of T_2.
[88]The author is indebted to Dr. J. L. Hall for applying his line-shape fitting program to some numerically generated data.
[89]Physically η cannot be changed without also changing β_0 or α, so it is important to specify which parameters are varied and which are held fixed.
[90]W. W. Rigrod, J. Appl. Phys. 34, 2602 (1963).
[91]W. B. Bridges, IEEE J. Quantum Electron. 4, 820 (1968).
[92]L. A. Ostrovskii and E. I. Yakubovich, Zh. Eksper. i Teor. Fiz. 46, 963 (1964) [Sov. Phys. JETP 19, 656 (1964)].
[93]W. W. Rigrod, J. Appl. Phys. 36, 2487 (1965).
[94]N. V. Karlov and Yu. B. Konev, Radio Eng. and Elect. Phys. 13, 491 (1968).
[95]F. Shimizu, Appl. Phys. Lett. 14, 378 (1969).
[96]The Doppler width of the laser is taken to be 1.54 times that of the absorber, corresponding to CO_2 laser radiation absorbed by SiF_4 [F. R. Petersen and B. L. Danielson, Bull. Am. Phys. Soc. 15, 1324 (1970)].
[97]O. N. Kompanets and V. S. Letokhov, Zh. Eksp. Teor. Fiz. Pis'ma Red. 14, 20 (1971)[JETP Lett. 14, 12 (1971)].

PHYSICAL REVIEW A VOLUME 8, NUMBER 1 JULY 1973

Liquid-Aluminum Structure Factor by Neutron Diffraction*

J. M. Stallard
Naval Ordnance Laboratory, Silver Spring, Maryland 20910

C. M. Davis, Jr.†
American University, Washington, D.C. 20016

(Received 4 January 1973)

The structure factor $S(Q)$ for liquid aluminum was measured at 703 and 1029 °C in the region $0 < Q < 15$ Å^{-1} using neutron-diffraction techniques. A description of the experimental apparatus and procedure is presented, as well as the method of reducing the neutron intensity to the structure factor. The results are compared with other simple liquid metals, and the electrical resistivity is calculated using the Ziman formulation. Excellent agreement is obtained between calculated and experimentally observed resistivity, both in absolute value and in temperature dependence. This agreement lends credence to both the measured structure factor and to the Ziman formulation for resistivity.

I. INTRODUCTION

Over the past decade highly successful statistical-mechanical approaches have been developed for predicting the properties of liquified inert gases.[1] Recently these techniques have been combined with various model potentials and used to calculate the thermodynamic and electrical properties of liquid metals.[2,3] In these calculations, the concept of a radial distribution function $g(r)$, or its transform, the structure factor $S(Q)$, and their temperature dependences are used. Neutron diffraction offers the most direct experimental means for obtaining the above quantities.

In the present investigation theories previously applied to the liquid alkali metals are extended to the case of a polyvalent liquid metal. The structure factor of liquid aluminum is obtained at 703 and 1029 °C. Aluminum was chosen for this study because it is a "simple" polyvalent monatomic liquid for which a great deal of experimental data is available. The results are used to predict the electrical resistivity and its temperature dependence.

II. EXPERIMENTAL DETAILS

Neutron-diffraction measurements were made at 703 and 1029 °C by transmission through a sample of aluminum contained in a cylindrical alumina crucible. The sample was prepared from a MRC VP grade (99.995% pure) aluminum rod. The crucible was 99.8% pure alumina (Coors CN-100) with a wall thickness of 0.176 cm and an inside radius of 1.80 cm. The effective sample height (neutron beam height) was 5.08 cm. Heating was accomplished by means of a cage-wound furnace element made of 0.020-in.-diam molybdenum wire (Fig. 1). Three concentric cylindrical cans fabricated from 0.005-in. molybdenum sheet served as heat radiation shields (Fig. 2). The vacuum fur-

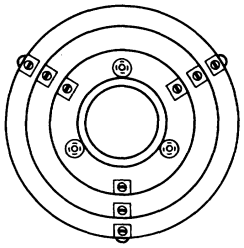

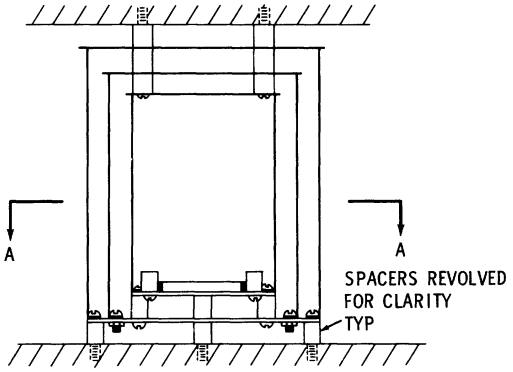

FIG. 2. Heat radiation shielding.

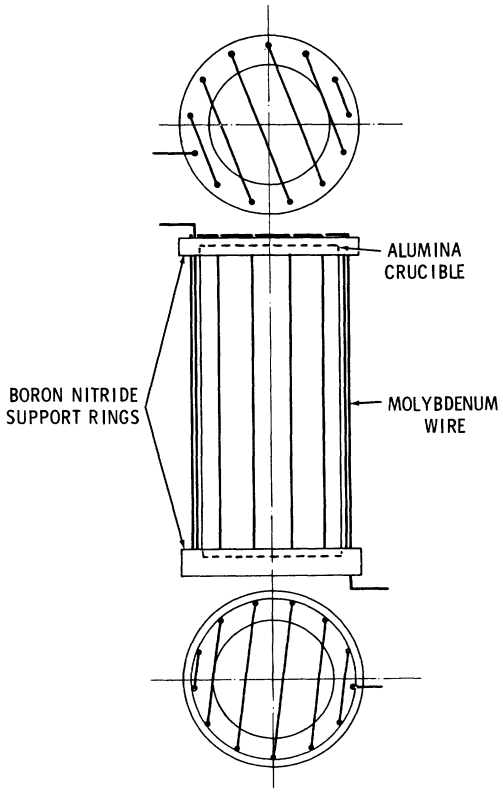

FIG. 1. Furnace element—crucible assembly.

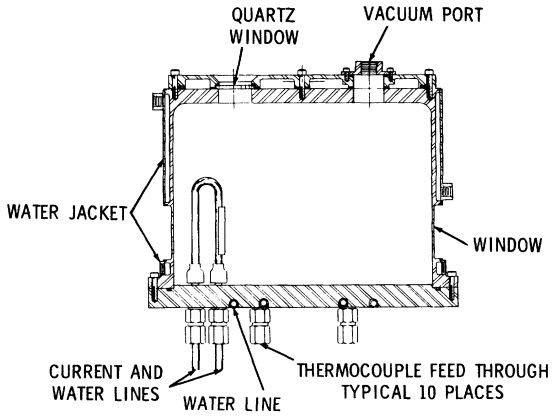

FIG. 3. Neutron furnace housing.

nace housing was constructed of aluminum. Published criteria for the construction of high-temperature furnaces[4-9] were employed where possible in the design of the present neutron furnace, which consisted of two main pieces, a cylindrical can, and a base plate, sealed together by an O ring (Fig. 3). Aluminum water jackets were welded around the can above and below the $\frac{1}{16}$-in.-thick aluminum neutron window. Another machined jacket was attached to the top of the can and sealed by an O ring. The base plate was cooled by a cooper-tubing configuration, silver soldered into the base. The top assembly was fitted with a quick-connect vacuum port and a quartz window. The base plate was provided with 14 Conax fittings, which were used to feed through thermocouples, current leads, etc. Standard techniques were used to maintain and measure the vacuum.

The temperature was monitored by means of a tantalum-sheathed tungsten, tungsten–26%-rhenium thermocouple located below the neutron window and outside of the crucible but inside the innermost heat shield and as close to the crucible as possible. Since the temperature probe was not located in the melt during the diffraction experiment, no structure from the probe itself was observed. During a separate temperature run, the monitor thermocouple was calibrated against a tungsten–3%-rhenium, tungsten–25%-rhenium thermocouple whose calibration certification is traceable to NBS. The latter thermocouple was centered in the test melt.

The present experiment was performed at the NBS neutron reactor.[10-12] The arrangement used for the crystal spectrometer measurements was similar to that described by Bacon.[13] Standard collimation procedures[14-16] were employed. Scattered neutrons were detected by means of a BF_3 proportional counter. A low efficiency He^3-gas-filled counter served as the monitor. Detailed descriptions of both types of counters are available.[17-20]

TABLE I. Experimental parameters.

Quantity	$T = 703$ °C	$T = 1029$ °C
$\lambda_{2.4}$(Å)	2.381	2.377
Q range (Å^{-1})	1.1–4.1	0.8–4.4
$\lambda_{1.0}$ (Å)	0.995	1.004
Q range (Å^{-1})	3.8–9.8	4.0–10.3
$\lambda_{0.7}$ (Å)	0.723	0.698
Q range (Å^{-1})	9.3–14.8	9.9–14.5
S (0)	0.0173	0.0263

In order to calculate the structure factor from the measured intensities over a wide range of momentum transfer Q, it was necessary to use three neutron wavelengths. The (0002) plane of a graphite crystal in reflection was used to provide 2.4-Å neutrons for the low-Q region. The (111) plane of a copper crystal in transmission was used to provide 1.0-Å neutrons in the intermediate region, and 0.7-Å neutrons for the region of high Q. For the 2.4-Å neutrons, higher orders were present but were eliminated by placing a 2-in.-thick pyrolytic graphite crystal, oriented with its c axis parallel to the beam path, between the monochromator and the monitor. This technique allowed approximately 70% of the 2.4-Å neutrons to pass while providing nearly total extinction of higher-order neutrons.

The exact neutron wavelength and counter-arm zero were determined by measuring the position of five well-resolved peaks of a copper powder sample. The maximum uncertainty in counter-arm position θ, was 0.005°. Table I summarizes the important parameters of the experiment.

III. DATA REDUCTION

The intensity due to the sample alone is not, in general, the simple subtraction of the two runs, with and without sample. In practice, both the incident and scattered beam are subject to absorption and scattering in the sample and in the crucible. The presence of the sample changes the intensity incident on the crucible. This change must be taken into account before a systematic subtraction of the data can be made.

The method for subtraction has been outlined by Pings and co-workers.[21,22] The result is

$$I(Q) = a(I_{sc}^{E} - bI_{c}^{E}), \tag{1}$$

where $I(Q)$ is the desired scattered intensity due to the sample, I_c^E and I_{sc}^E are the experimentally measured intensities, without and with sample, respectively, and a and b are constants for a given value of Q which are determined by the geometry of the experiment. (In the present work, the method of Pings *et al.* is modified slightly in order to yield scattering elements of equal volume, in the numerical integration necessary to produce the constants a and b.)

Except in the region of small Q where I_{sc}^E and bI_c^E are approximately equal, errors due to count-

ing statistics are kept small by counting for sufficiently long periods. Large errors do occur in the vicinity of elastic peaks arising from the aluima crucible. The chemical reactivity of liquid aluminum prevented the use of an isotropic scatterer such as vanadium for the sample container. Ceramic materials, while chemically inert, are not isotropic scatterers. The practical solution used in this experiment was to smooth the subtracted curve in the vicinity of the alumina peaks.

In the neutron-diffraction experiment the sample is irradiated by monoenergetic neutrons of wavelength λ. The observed intensity $I(Q)$ is the intensity at a particular scattering angle, which includes primary and multiple scattering events as well as an integrated intensity over all energy transfers due to inelastic scattering. Also, the intensity depends on the efficiency of the detection system, which is, in general, Q dependent. Following the method of Enderby,[23] and assuming coherent scattering in aluminum, one obtains the structure factor $S(Q)$ from the measured intensity $I(Q)$ by

$$S(Q) = C(\lambda)I(Q) - f(Q) - M(Q). \tag{2}$$

In Eq. (2), $I(Q)$ is the measured intensity of scattered neutrons, $C(\lambda)$ is a normalization constant, $f(Q)$ is a correction for inelastic scattering, and $M(Q)$ is a correction for multiple scattering. To obtain the structure factor, it is only necessary to evaluate $C(\lambda)$, $f(Q)$, and $M(Q)$.

It is known that as Q becomes large, $S(Q)$ approaches unity. This fact was used to calculate $C(\lambda)$ for the short-wavelength run. Intensity measurements were made to sufficiently large Q such that no structure was seen. Unity was substituted for $S(Q)$ and calculated values were inserted for $f(Q)$ and $M(Q)$ in Eq. (2). Then $C(\lambda)$ was that number that yielded the observed intensity.

The Q ranges of the three different runs at a given temperature were chosen so as to have ample overlap between adjacent runs. In the overlap regions the calculated values of $f(Q)$ and $M(Q)$ were inserted along with the observed values of $I(Q)$. Then the $C(\lambda)$'s for the intermediate and long-wavelength runs were chosen so that in the regions of overlap, values for $S(Q)$ from two overlapping runs were the same. A few selected values of the product $C(\lambda)I(Q)$ are given in Table II.

The inelastic correction first introduced by Placzek,[24] and outlined in detail by Enderby,[23] contains a parameter m, whose value is 1 for a constant efficiency counter and 2 for a counter whose efficiency goes as the neutron wavelength. [Enderby's Eq. (32) gives $f(Q)$ as a function of the average kinetic energy of the atoms, the incident energy of the neutron, the ratio of nuclear to neutron mass, and m.] Actually, neither is the case. In practice the efficiency ϵ is given by

$$\epsilon = 1 - e^{-\mu_a L}, \tag{3}$$

where μ_a is the absorption attenuation coefficient and L is the length of the counter. Hughes and Schwartz[25] show that the absorption cross section in barns for B^{10} is given by

$$\sigma_a \approx 610.31/\sqrt{E_0}, \tag{4}$$

where E_0 is given in eV. But for neutrons,[26]

$$\lambda = 0.28600/\sqrt{E_0}, \tag{5}$$

where λ is in angstroms. Therefore,

$$\sigma_a = 2134.0\lambda. \tag{6}$$

The counter used was 12.750 in. (32.385 cm) long and was filled to 76 cm Hg pressure with BF_3 gas enriched to 96% B^{10}. Combining this information with Eqs. (3) and (6) yields

$$\epsilon = 1 - e^{-1.7762\lambda}. \tag{7}$$

Thus for a given counter

$$\epsilon = 1 - e^{-\alpha\lambda}, \tag{8}$$

where α is a constant. It is seen that, indeed, as λ gets small

$$\epsilon \simeq \alpha\lambda \tag{9}$$

and as λ gets large

$$\epsilon \simeq 1. \tag{10}$$

But for normal λ, ϵ is neither constant nor proportional to λ; m is neither 1 nor 2 but somewhere in between. The value for m, then, is calculated by

$$m = 2\epsilon/(\epsilon + \epsilon_0), \tag{11}$$

where ϵ_0 is defined as the ϵ intercept of the tangent to Eq. (8) at the value of λ being considered.

TABLE II. Selected values of data-reduction parameters.

Q	$C(\lambda)I(Q)$	$f(Q)$	$M(Q)$
	$T = 703$ °C		
1.1	0.314	0.103	0.191
2.67	2.281	0.072	0.034
4.9	1.396	0.001	0.064
14.5	1.005	−0.069	0.066
	$T = 1029$ °C		
1.1	0.373	0.139	0.179
2.67	2.038	0.108	0.051
4.9	1.306	0.007	0.065
14.5	1.007	−0.060	0.066

A few selected values of $f(Q)$, calculated from Enderby's[23] formula and Eq. (11), are given in Table II.

The determination of the structure factor $S(Q)$ depends on measuring single-scattering events. However, because the sample material has finite thickness, double- and higher-order scattering is always present. Vineyard[27] considered plane samples of infinite lateral extent and assumed isotropic scattering by the sample. Brockhouse *et al.*[28] checked Vineyard's calculations experimentally for several coherent scatterers and found only reasonable agreement. Blech and Averbach[29] made calculations for a cylindrical incoherent scatterer and checked these calculations experimentally in vanadium (an incoherent scatterer) and copper (a coherent scatterer). The calculations predicted the vanadium results but underestimated the copper results. Cocking and Heard[30] considered plane samples of finite lateral extent using the known or assumed angular distribution of primary scattering. All the above calculations assumed elastic scattering and derived results only for secondary scattering. They assumed that if $I_2/\bar{I}_1$, the ratio of secondary to primary scattering, is small, then

$$\frac{I_{n+1}}{I_n}=\frac{I_2}{\bar{I}_1}, \tag{12}$$

where $\bar{I}_1$ is equal to I_1 if $S(Q)$ is equal to 1. Therefore, the multiple scattering intensity I_M, defined as second order and higher scattering, is given by

$$I_M=I_2/(1-I_2/\bar{I}_1). \tag{13}$$

In this experiment, multiple scattering was calculated for a cylindrical sample using the angular distribution of primary scattered neutrons in the calculations. The observed intensity itself was used as an approximation to the primary scattering. Equation (12) was assumed to apply.

The number of neutrons per unit solid angle scattered from a volume dV for an incoming flux J_0 is given by

$$I_1(Q)=\frac{J_0\sigma_s N_v}{4\pi}S(Q)\int e^{-\mu(L_1+L_2)}dV, \tag{14}$$

where σ_s is the scattering cross section, N_v is the atomic density of the sample, L_1 (L_2) is the distance the neutron travels in the sample before (after) scattering, and μ is the total attenuation coefficient of the sample. The secondary scattering is given by

$$I_2(Q)=\frac{J_0\sigma_s^2N_v^2}{16\pi^2}\times\int\frac{e^{-\mu(L_1+L+L_2)}}{L^2}S(Q_1)S(Q_2)\,dV_1\,dV_2, \tag{15}$$

where L is the distance between the two scattering volumes dV_1 and dV_2, and $S(Q_1)$ and $S(Q_2)$ are the evaluations of the structure factor for the first and second scatterings.

The ratio of primary to total scattering $R(Q)$, defined by

$$R(Q)=\frac{I_1(Q)}{I_1(Q)+I_M(Q)}, \tag{16}$$

is more convenient since calculating this number obviates normalization problems. Substituting Eq. (16) into Eq. (2) and solving for $M(Q)$ yields

$$M(Q)=\frac{[S(Q)+f(Q)][1-R(Q)]}{R(Q)}. \tag{17}$$

It should be noted that it is necessary to know $S(Q)$ in order to calculate $I_1(Q)$, $I_2(Q)$, and $M(Q)$. An estimate of $S(Q)$ was obtained in the following manner. First, the three runs at a given temperature, with different neutron wavelengths, were normalized, one to another. Then the approximation was made that $M(Q)$ and $f(Q)$ are constants. Under this approximation, Eq. (2) is linear,

$$I(Q)=aS(Q)+b. \tag{18}$$

The constants a and b are evaluated by considering the two limiting values of $S(Q)$. It is known[3] that as Q becomes small, $S(Q)$ becomes proportional to the isothermal compressibility κ_T,

$$\lim_{Q\to 0}S(Q)=N_v k_B T\kappa_T, \tag{19}$$

where k_B is Boltzmann's constant and T is temperature. Values for $S(0)$ were calculated using values from the literature for N_v[31, 32] and κ_T,[33] and measured values for T. It is also known that

$$\lim_{Q\to\infty}S(Q)=1. \tag{20}$$

Thus Eq. (18) becomes

$$S(Q)\approx\frac{I(Q)[1-S(0)]-I(0)+I(\infty)S(0)}{I(\infty)-I(0)}. \tag{21}$$

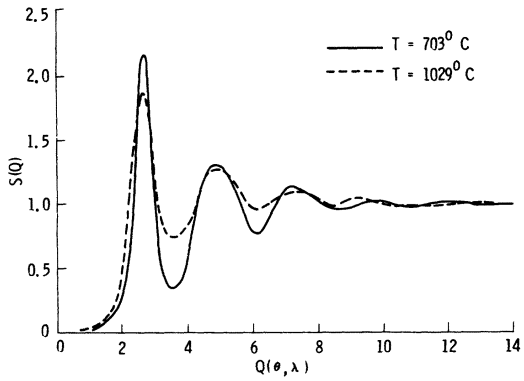

FIG. 4. Structure factor for liquid aluminum.

TABLE III. Structure factor for liquid aluminum at 703 °C.

Q	0.0	0.1	0.2	0.3	0.4	0.5	0.6	0.7	0.8	0.9
0										
1		0.020	0.026	0.040	0.058	0.071	0.097	0.127	0.148	0.223
2	0.295	0.400	0.557	0.779	1.134	1.663	2.078	2.153	1.986	1.447
3	(1.104)	0.760	0.586	0.436	0.368	0.352	0.330	0.363	(0.410)	0.458
4	(0.505)	(0.658)	(0.802)	(0.930)	1.043	(1.136)	(1.213)	1.273	1.343	1.331
5	(1.327)	1.345	1.254	1.215	1.147	(1.099)	1.018	0.947	0.901	0.828
6	0.801	0.766	0.789	0.825	0.853	0.870	0.924	0.977	1.027	1.055
7	1.089	1.131	1.127	1.160	1.149	1.111	1.098	1.119	1.087	1.042
8	0.998	0.991	0.985	0.972	0.966	0.936	0.947	0.963	0.964	0.966
9	0.986	0.990	0.994	0.995	1.006	1.013	1.025	1.034	1.041	1.021
10	1.017	1.006	1.005	1.002	0.997	0.986	0.977	0.970	0.965	0.970
11	0.974	0.976	0.979	0.986	0.989	0.993	0.999	1.002	1.004	1.006
12	1.004	1.007	1.006	1.006	1.007	0.997	0.998	0.999	1.003	0.995
13	0.995	0.997	0.995	0.994	0.998	1.003	0.996	0.996	1.001	1.002
14	1.005	1.012	1.004	1.007	1.008	1.008	1.008	1.006	1.019	

$S(2.67) = 2.175$

The necessary ingredients for the calculation of $I_1(Q)$, $I_2(Q)$, and $M(Q)$ have been obtained. Details of the calculations of Eqs. (14) and (15) are given elsewhere.[34] A few selected values of $M(Q)$ are given in Table II.

Experimental values for the structure factor for liquid aluminum, determined from scattered neutron intensity and the calculated corrections of Eq. (2), are given in Tables III and IV at 703 and 1029 °C, respectively. The values in parentheses lie in the regions of large alumina peaks and have been smoothed. Figure 4 shows least-square fits to the experimental data, used to obtain the values in parentheses in Tables III and IV. The curves are spline functions consisting of cubics whose first and second derivatives are equal where joined. It is estimated that errors in the experimental data are about 1% for large Q and about 0.5% at the peak value. The error at very small Q increases rapidly with decreasing Q.

The error in a given Q value, estimated from uncertainties in λ and θ is approximately 0.005 Å^{-1} at the largest λ and smallest θ, and 0.02 Å^{-1} at the smallest λ and largest θ.

IV. DISCUSSION

Simple liquid metals are characterized by the symmetry of the main peak of the structure factor.[2,3] Larsson *et al.*[35] observed that the structure factor for liquid aluminum at 677 °C was indeed symmetrical in the region of the main peak. In the present work the same symmetry is observed. Table V

TABLE IV. Structure factor for liquid aluminum at 1029 °C.

Q	0.0	0.1	0.2	0.3	0.4	0.5	0.6	0.7	0.8	0.9
0									0.039	0.045
1	0.047	0.055	0.066	0.084	0.106	0.132	0.165	0.219	0.271	0.376
2	0.486	0.632	0.821	1.076	1.372	1.670	1.821	1.833	1.629	(1.568)
3	(1.375)	(1.159)	0.910	0.822	(0.678)	(0.641)	(0.653)	(0.698)	0.736	(0.811)
4	0.818	0.869	0.934	0.977	1.010	1.070	1.176	1.261	1.259	1.234
5	1.245	1.327	1.320	1.242	1.154	1.098	1.054	1.037	1.037	1.009
6	0.975	0.958	0.956	0.980	1.008	1.015	1.020	1.030	1.057	1.077
7	1.090	1.084	1.085	1.091	1.094	1.077	1.072	1.083	1.077	1.065
8	1.046	1.026	1.024	1.016	0.994	0.993	0.998	1.017	1.022	1.023
9	1.035	1.037	1.042	1.037	1.029	1.015	1.014	1.016	1.024	1.024
10	1.020	1.014	1.006	1.003	1.003	0.998	0.999	0.993	0.997	0.991
11	0.993	0.991	0.994	0.994	0.995	0.992	0.993	0.994	0.990	0.995
12	1.002	1.005	1.003	1.007	1.005	1.005	1.002	1.000	1.004	0.996
13	1.001	0.999	1.000	0.998	0.991	0.993	1.000	0.996	1.002	1.000
14	1.006	1.004	1.007	1.005	1.004	1.001				

$S(2.67) = 1.879$

shows a detailed comparison of peak and valley positions and intensities between the Larsson data at 677 °C and the present work at 703 °C. The positions of the peaks and valleys and the general features of the curves are in agreement. The only noticeable difference is the depth of the first minimum. The minimum in the present work is somewhat deeper than Larsson's and that of other simple liquid metals near the melting point.

Egelstaff *et al.*[36] performed a careful experiment, specifically designed to measure the structure factor of several liquid metals in the difficult low-Q region $0.2 < Q < 1.6$ Å^{-1}. Table VI compares the present results at 703 °C and their results for aluminum just above melting (660 °C) in the Q region where the two sets of data overlap. While the agreement is probably fortuitous because of large errors in the low-Q data of the present work, it is nevertheless encouraging.

Okazaki *et al.*[37] reported structure-factor data for liquid aluminum at 670, 770, and 870 °C. Their largest Q value is 5.2 Å^{-1} and it is not clear how their data have been normalized. Contrary to all other available data they report a "smoothed hill on the left-hand side of the first main peak" and a "shoulderlike trace on the right-hand side of the first main peak." Comparison with the data of Egelstaff *et al.*, Larsson *et al.*, and the present work tends to discount the data of Okazaki *et al.*

It is interesting to compare the present aluminum data to those of other simple liquid metals. Ashcroft and Lekner[38] noted that

$$S_{\max}(Q) \simeq 2.5 \tag{22}$$

for all simple liquid metals at the melting temperature. They also observed that if the wave number Q is scaled by a factor proportional to the interatomic distance ($\sim Q/N_v^{1/3}$), the positions of the first peak for simple liquid metals coincide. With these two observations in mind, they proceeded to calculate the structure factor for a hard-sphere model that depends on one parameter, the

TABLE V. Comparison with Larsson *et al.* (Ref. 35).

	Q (Å^{-1})		$S(Q)$	
	Larsson *et al.*	Present work	Larsson *et al.*	Present work
First max	2.70	2.67	2.20	2.17
First min	3.61	3.63	0.55	0.33
Second max	4.86	4.94	1.22	1.33
Second min	6.16	6.14	0.87	0.77
Third max	7.30	7.32	1.18	1.15

TABLE VI. Comparison with Egelstaff *et al.* (Ref. 36).

	$S(Q)$	
Q	Egelstaff *et al.*	Present work
1.27	0.02	0.04
1.50	0.02	0.07
1.73	0.08	0.13

packing fraction, given by

$$\eta = \tfrac{1}{6}\pi N_v \sigma^3, \tag{23}$$

where σ is the hard-sphere diameter. They found that for $\eta = 0.45$, the hard-sphere model predicts both the position and the height of the first peak in the structure factor of simple liquid metals. This observation suggests that at melting, all simple liquid metals have a similar structure, viz., that of a hard-sphere fluid with a packing fraction of 0.45. The present aluminum data at 703 °C compare very well with those of the hard-sphere model. The value of $Q_0/N_v^{1/3}$ for aluminum is 7.1, while that for the hard-sphere model is 7.0, where Q_0 is the position of $S_{\max}$. $S_{\max}$ for the aluminum is 2.2 while that for the hard sphere is 2.5.

Schiff[39] has extended the hard-sphere analysis to include each peak and valley of the structure-factor curve, just above the melting temperature. He picks a packing fraction η_n such that the amplitude of the nth peak or valley for the hard-sphere fluid exactly equals that of the actual liquid. The successive η's decrease monotonically because the initial rise of the radial distribution function $g(r)$ is less abrupt than in the hard-sphere case. The faster the decrease in η, therefore, the softer the interatomic potential. Table VII compares Schiff's analysis of the x-ray data of Fessler *et al.*[40] for liquid aluminum at 665 °C and an analysis of the

TABLE VII. Packing fraction that matches the structure factor of a hard-sphere fluid to that of the actual liquid at the given extremum. The values of the packing fraction for all but the present work are taken from Ref. 39.

	1st peak	1st valley	2nd peak	2nd valley	3rd peak
Sodium (Ref. 41)	0.45	0.44	0.41	0.3	0.25
Lead (Ref. 42)	0.47	0.47	0.44	0.42	0.41
Aluminum (Ref. 40)	0.45	0.49	0.43	0.40	0.36
Aluminum (present work)	0.42	>0.51[a]	0.46	0.51	0.47

[a] Packing fractions >0.51 were not available.

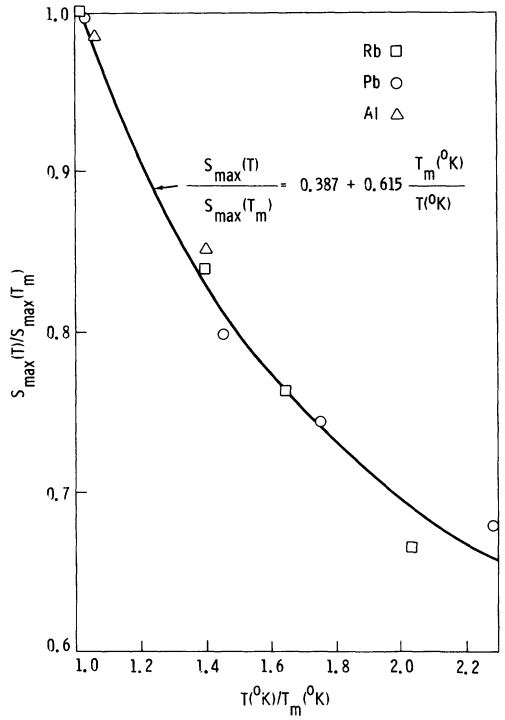

FIG. 5. Temperature dependence of $S_{max}(Q)$ for simple liquid metals.

present work at 703 °C. Table VII also shows, for comparison, Schiff's treatment for sodium and lead.[41,42] Contrary to the results obtained from Fessler *et al.*, the present results indicate a relatively constant packing fraction through the third peak and suggest that the repulsive part of the ion-ion potential for liquid aluminum is more closely approximated by a hard-sphere potential than are the potentials of sodium and lead.

Examination of Fig. 4 shows that as the temperature increases, the peaks and valleys of the structure factor broaden considerably, the peaks losing intensity and the valleys becoming more shallow. This phenomenon is due to the increase in random thermal motion of the ions with temperature. It is noted empirically that if the temperature is scaled to the melting temperature, then S_{max} for the present aluminum data and those for rubidium[41] and lead[43] all have the same temperature dependence (Fig. 5).

Finally, the present structure-factor data were used to calculate the electrical resistivity of liquid aluminum using the Ziman[44] formula and an optimized model potential proposed by Shaw and Pynn.[45] The Shaw potential is very carefully developed from spectroscopic data, taking into account screening in a way that includes exchange and correlation effects. It has no adjustable parameters. In the low-Q region, where there are no data in the present work, a straight-line extrapolation to $S(0)$, calculated from the isothermal compressibility, is used. Table VIII gives the results of the calculation and compares these values to experimentally measured values.[46] As can be seen, the agreement is excellent, in both absolute value and in temperature dependence.

TABLE VIII. Resistivity of liquid aluminum.

	Experimental (Ref. 46)	Calculated
ρ_{703} ($\mu\Omega$ cm)	24.8	26.6
ρ_{1029} ($\mu\Omega$ cm)	29.6	32.3
$\frac{d\rho}{dT}$ ($\mu\Omega$ cm/°C)	0.0148	0.0179

There has been some discussion in the literature[47] of the validity of the Ziman formulation for resistivity. There are many approximations in its derivation and relatively small changes in input data can significantly alter the calculated values of resistivity. It can only be said that as experimental data for $S(Q)$ improve, and as proposed model potentials become more realistic, the Ziman formula continues to yield good results. The present calculations using the measured structure factor and the Shaw potential are quite good, lending support to both the experimental structure-factor data and the Ziman formula for resistivity.

ACKNOWLEDGMENTS

The authors wish to thank Bernard Mozer who supplied furnace drawings upon which the design of the present furnace housing is based. Stanley Pickart and Harvey Alperin gave freely of their knowledge and experience in neutron-diffraction techniques. Finally, we would thank Neil Brown, who made the resistivity calculations, and Jacek Jarzynski for many discussions concerning the theory of liquid metals.

*Paper based on a dissertation submitted by J. M. Stallard to The American University in partial fulfillment of requirements for a Ph.D. degree. A beam port for the experiment was supplied free of charge by the The National Bureau of Standards at their neutron reactor.

†Present address: The Naval Research Laboratory, Washington, D.C.

[1] *Physics of Simple Liquids*, edited by H. Temperley, J.

Rowlinson, and G. Rushbrooke (North-Holland, Amsterdam, 1968).
[2]N. H. March, *Liquid Metals* (Pergamon, London, 1968).
[3]P. A. Egelstaff, *An Introduction to the Liquid State* (Academic, London, 1967).
[4]A. U. Seybolt and J. E. Burke, *Procedures in Experimental Metallurgy* (Wiley, New York, 1953).
[5]R. Kieffer and F. Benesovsky, Metallurgia **58**, 1 (1958).
[6]C. W. Haworth and W. Hume-Rothery, J. Inst. Met. **87**, 265 (1958).
[7]C. W. Haworth, J. Less-Common Met. **1**, 106 (1959).
[8]E. V. Kornelsen and J. O. Weeks, Rev. Sci. Instrum. **30**, 290 (1959).
[9]J. Cohen and W. Eaton, Rev. Sci. Instrum. **31**, 522 (1960).
[10]Natl. Bur. Stds. Report No. 8993 (NBSR 9), 1966 (unpublished).
[11]Natl. Bur. Stds. Report No. 9419 (NBSR 9A), 1966 (unpublished).
[12]Natl. Bur. Stds. Report No. 9081 (NBSR 10), 1966 (unpublished).
[13]G. E. Bacon, *Neutron Diffraction* (Oxford U. P., London, 1962).
[14]V. L. Sailor, H. L. Foote, Jr., H. H. Landon, and R. E. Wood, Rev. Sci. Instrum. **27**, 26 (1956).
[15]G. Caglioti, A. Paoletti, and F. P. Ricci, Nucl. Instrum. **3**, 223 (1958).
[16]B. T. M. Willis, Acta Crystallogr. **13**, 763 (1960).
[17]I. L. Fowler and P. R. Tunnicliffe, Rev. Sci. Instrum. **21**, 734 (1950).
[18]W. Abson, P. G. Salmon, and S. Pyrah, Proc. IEEE **105B**, 357 (1958).
[19]W. D. Allen, *Neutron Detection* (Philosophical Library, New York, 1960).
[20]S. J. Cocking and F. J. Webb, in *Thermal Neutron Scattering*, edited by P. A. Egelstaff (Academic, London, 1965).
[21]H. H. Paalman and C. J. Pings, J. Appl. Phys. **33**, 2635 (1962).
[22]A. P. Kendig and C. J. Pings, J. Appl. Phys. **36**, 1692 (1965).
[23]J. E. Enderby, in *Physics of Simple Liquids*, edited by H. N. V. Temperly, J. S. Rowlinson, and G. S. Rushbrooke (North-Holland, Amsterdam, 1968).
[24]G. Placzek, Phys. Rev. **86**, 377 (1952).
[25]D. J. Hughes and R. B. Schwartz, *Neutron Cross Sections* (U.S. GPO, Washington, D.C., 1958).
[26]R. D. Evans, *The Atomic Nucleus* (McGraw-Hill, New York, 1955).
[27]G. H. Vineyard, Phys. Rev. **96**, 93 (1954).
[28]B. N. Brockhouse, L. M. Corliss, and J. M. Hastings, Phys. Rev. **98**, 1721 (1955).
[29]I. A. Blech and B. L. Averbach, Phys. Rev. 137, A1113 (1965).
[30]S. J. Cocking and C. R. T. Heard, Atomic Energy Research Establishment Report No. R5016, 1965 (unpublished).
[31]E. Gebhardt, M. Becker, and A. Dorner, Z. Metallkd. **44**, 573 (1953).
[32]E. I. Gol'tsova, High Temp. **3**, 438 (1965).
[33]H. J. Seeman and F. K. Klein, Z. Angew. Phys. **19**, 368 (1965).
[34]J. M. Stallard, Naval Ordnance Technical Laboratory Report No. 71-142, 1971 (unpublished).
[35]K. E. Larsson, U. Dahlborg, and D. Jovic, in *Proceedings of the Symposium on Inelastic Scattering of Neutrons* (International Atomic Energy Agency, Vienna, 1964), Vol. 2.
[36]P. A. Egelstaff, C. Duffill, V. Rainey, J. E. Enderby, and D. M. North, Phys. Lett. **21**, 286 (1966).
[37]H. Okazaki, K. Iida, and S. Tamaki, J. Phys. Soc. Jap. **29**, 1396 (1970).
[38]N. W. Ashcroft and J. Lekner, Phys. Rev. **145**, 83 (1966).
[39]D. Schiff, Phys. Rev. **186**, 151 (1969).
[40]R. R. Fessler, R. Kaplow, and B. L. Averbach, Phys. Rev. **150**, 34 (1966).
[41]N. S. Gingrich and L. Heaton, J. Chem. Phys. **34**, 873 (1961).
[42]R. Kaplow, S. L. Strong, and B. L. Averbach, Phys. Rev. **138**, A1336 (1965).
[43]D. M. North, J. E. Enderby, and P. A. Egelstaff, J. Phys. C **1**, 1075 (1968).
[44]J. M. Ziman, Adv. Phys. **13**, 89 (1965).
[45]R. W. Shaw, Jr. and R. Pynn, J. Phys. C **2**, 2071 (1969).
[46]A. Roll and H. Motz, Z. Metallkd. **48**, 272 (1957).
[47]A. J. Greenfield, Phys. Rev. Lett. **16**, 6 (1966).

PHYSICAL REVIEW A VOLUME 8, NUMBER 1 JULY 1973

Multiple-Scattering Correction to Transport Coefficients of He^3-He^4 Mixtures

C. S. Hsu
Department of Physics, Columbia University, New York, New York 10027
Bell Telephone Laboratories, Murray Hill, New Jersey 07974
(Received 13 April 1972)

In McMillan's first-order calculation, the transport coefficients obtained are a factor of 2 too large. Here we do the calculation by including the multiple-scattering contribution. By carefully picking the cutoff, we get a good agreement with experiment.

I. INTRODUCTION

Recently, McMillan[1,2] has used microscopic theory to calculate the transport coefficients of He^3 in liquid He^4. In his calculation the parameter α, the deformation potential coupling of one He^3 quasiparticle to He^4 phonons, was chosen to fit one transport coefficient and had the value $\alpha = 0.24$. With this value, the theoretical transport coefficients are in reasonably good agreement with experiment. However, Edwards has pointed out that there is a thermodynamic relation between the